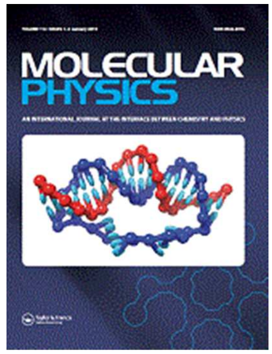

Nonlinear Dynamics of Dipoles in Microwave Electric Field of a Nanocoaxial Tubular Reactor

Journal:	*Molecular Physics*
Manuscript ID	Draft
Manuscript Type:	Full Paper
Date Submitted by the Author:	n/a
Complete List of Authors:	Kapranov, Sergey; Norwegian University of Science and Technology, Electronic Systems Kouzaev, Guennadi; Norwegian University of Scievce and Technology, Department of Electronic Systems
Keywords:	nanocoax reactor, AC electric field gradient force, nonlinear dynamics, dipole

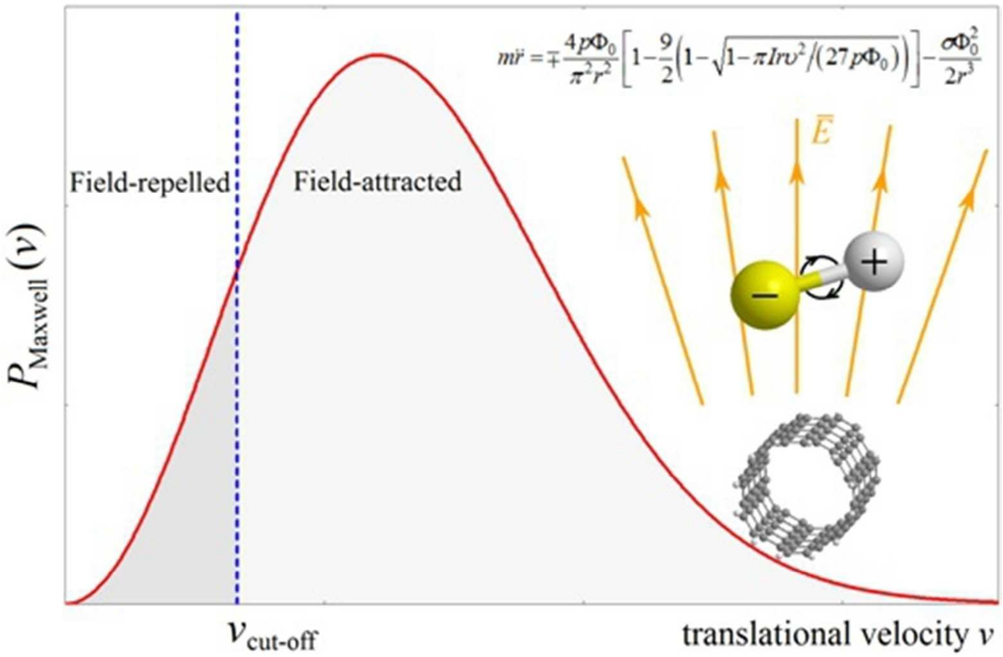

137x90mm (96 x 96 DPI)

This semi-analytical work is to discover the unknown earlier peculiarities of dipole motion in a nano-manufactured coaxials interesting in molecular sensing, spectroscopy, and nanochemistry. The applied alternating high-gradient electric field is for rotating and acceleration of dipoles towards or away from the central nanoconductor with the aim of increasing the rate of chemical reactions. The given theory allows finding the parameters of electric field and reactor geometry for the effective pumping of the field energy to the thermalized dipoles. Given approach is allowed, as well, for classical dipole motion calculations in infrared and visible lights and plasmonic waves.

Nonlinear Dynamics of Dipoles in Microwave Electric Field of a Nanocoaxial Tubular Reactor

Sergey V. Kapranov[a], Guennadi A. Kouzaev[b]

Department of Electronic Systems, Norwegian University of Science and Technology – NTNU, Trondheim, Norway

O.S. Bragstads plass 2B, Gløshaugen, 7491 Trondheim, Norway

[a] E-mail: sergey.v.kapranov@yandex.ru

[b] Corresponding author; e-mail: guennadi.kouzaev@ntnu.no

Nonlinear Dynamics of Dipoles in Microwave Electric Field of a Nanocoaxial Tubular Reactor

A novel analytical pseudo-nonadiabatic approach to dynamics of rotating dipolar molecules in high-gradient microwave electric fields and applications for manipulating molecules in hollow coaxial nanoreactors are considered. The translational and rotational equations of motion of a dipole in the electric and surface potentials of a nanocoax are derived using the Euler-Lagrange theorem, and their semi-analytical modifications are proposed for expediting simulations. The Maxwell distribution of initial velocities of dipoles is adopted in the simulations to take into account the effect of temperature. Using the developed approach, the translational and rotational dynamics of thermalised dipoles in the high-gradient alternating electric field of the nanocoaxial cell are studied. A relationship for the alternating field gradient force acting on the rotating dipole is derived. The regimes of attraction and repulsion of dipoles near the central nanoconductor are discovered and are shown to differently affect the translational and rotational velocities of the dipoles. The conditions for these two dynamical regimes are analytically found. The developed model and obtained results are applicable for modelling the dynamics of both 'hot' and 'cooled' dipoles in promising electrically-controlled coaxial and multiwire nanoreactors, chemical sensors, and in new molecular spectroscopes proposed in this contribution.

Keywords: coaxial nanocable, nanocoax, AC field gradient force, nonlinear dynamics, dipole

1. Introduction

Manipulation of particles, molecules, and atoms on nanoscale has opened many intriguing possibilities in chemistry, molecular sensing, and nanomedicine [1]-[5]. The key reason is that in nanosized volumes the walls of the reactor influence the energy profiles of reactions, and even the reactions with high activation energy, which do not occur at given temperatures, can proceed [2]. Applying microwave electric fields can additionally accelerate reactions on these surfaces [6]. Besides, the confined conditions restrict the orientation of molecules so that probability of some non-conventional reaction pathways increases and the target product can form interesting spatial structures and have physicochemical properties different from those of the same product obtained in open-vessel conditions [7].

The nanoreactors are the hollow protein globules [5], [7]-[12] and many other nanostructures of tubular shape [2], [7]. These reactors are controlled chemically or electrically, e.g., by varying the transmissivity of walls or destroying them for the release of products [8], [11]-[13]. Small size of reactors allows applying high-gradient electric fields to the reactor walls at low voltage, and these fields may affect, for instance, the process of folding and unfolding of protein globules [13]-[17]. Trapping molecules or nanoparticles at room temperature in liquids is more challenging in comparison with confining ultracold atoms [18], [19], and combination of laser light with electrophoretic forces allows trapping nanoparticles in an adaptive manner in nano- or microtraps [20], [21].

Special attention is paid to tubular nanoreactors for manipulation of particles and nanodroplets in the continuous-flow regime. These reactors include single- or multi-walled carbon nanotubes or nanotubes of other materials [1], [2], [7], [22], [23]. These tubes are loaded with molecules typically using osmotic mechanisms, but the electric field can be used for this purpose as well [24]-[27]. Many works are focused on carrying out heterogeneous reactions in carbon nanotubes where the catalytic particles together with the wall material can increase the chemical reaction rates by several times [2], [3], [9], [10]. N-doped carbon nanotubes in a coaxial design can work also as electrocatalysts [28] and as supports for electrocatalytic single metal atoms [29].

Some nanotubes can be filled with nanoporous or semiconductor materials, and these tubes are used in highly sensitive electrically-based sensors of molecules [30].

Filling of nanotubes with photosensitive molecules can improve the characteristics of optical sensors [31].

Coaxial-based structures (Figure 1) as the multi-walled carbon nanotubes and micro-machined coaxial shells have found many applications in sensors and research cells [29], [32]-[36], in particular for studying the electrically-induced protein unfolding [2]. Earlier, coaxial reactors have found applications in minifludic microwave-assisted heating and chemical experimentations [37]. The convenience of these elements is in possibility of applying transverse DC/RF (Direct Current/Radio-Frequency) electric fields and obtaining large sensing response using simple instrumentation. For instance, the coaxial sensors demonstrate the sensitivity improvement by two orders of magnitude as compared with planar ones, and even few molecules moving along the sensor volume can be detected [35], [38].

Because of the small diameter of these coaxial cells, the intensity of electric field inside the nanocoax can be strong even at low voltage between the conductors and comparable with those of intermolecular fields, which allows manipulation of the molecules and intermolecular coupling.

Coaxial waveguides support propagation of not only microwaves, but also optical wavelengths including the hybrid optical-plasmon modes, and they are prospective for nanocommunications and fabrication of nanosemiconductor active components and nanosensors. The coaxial design will enable integrating the sealed chemical parts with semiconductor sensing and energy-harvesting components [33]-[36], [38]-[41] and building advanced sensors and reactors with the combined control of chemical reactions by microwaves, optical and plasmon fields and strong DC voltages.

With a multitude of experimental results accumulated, the theoretical studies and creation of applied engineering algorithms and models of nanocomponents, and particularly coaxial-based ones, are yet in great demand. The difficulties arising in this area are typical for many multiphysical problems. In particular, electromagnetics should be coupled with particle dynamics, heat and fluid flow physics, stochastical dynamics, and quantum-mechanical effects. Ab initio or hybrid quantum mechanics/molecular mechanics computations can be applied directly to molecules in nanoreactors, but hours of computation time are required to simulate molecular dynamics on computers with several thousand CPU cores [42]. Besides the quantum computations, the classical and semi-classical methods can be applied to simulate molecular dynamics in external electric fields [43]-[45].

In this paper, we propose a semi-analytical approach for predicting dynamics of non-interacting dipoles in strongly non-uniform electric field near the inner nanoconductor of a nanocoaxial cell. Our interest in this type of dynamics is inspired by the well-known and efficient application of microwave fields in heating of liquids and solids for chemical synthesis [46], with the heat produced by rotation of dipolar molecules and their chaotic interactions with each other [47], [48]. Polar gases are less efficiently heated by microwaves due to long free paths of their molecules and relatively low intensity of the fields excited in large vessels [49]. In contrast, the intensity of electric field in nanoreactors can be so high that not only strong microwave heating can be achieved due to thermalisation of the partially field-oriented molecules [50], but also the molecules can be stretched, unfolded, transformed to ions, or be guided along certain trajectories by the field gradient force. In nanocoaxial cells, all these effects can be employed to manipulate non-interacting molecules.

In this work, using our semi-analytical model and numerical algorithms, we study the dynamics of a non-ionised polarisable dipole in the non-uniform microwave electric field of a coaxial cell near its central nanoconductor for possible engineering of some prospective components (such as sensors and nanoreactors) for manipulating neutral molecules. To take into account the thermal influence, the statistical averaging of the simulated dynamic characteristics is performed.

The paper is organised as follows. In Section 2, we present a model of a dipolar molecule traveling in the strongly non-uniform alternating (AC) field of a coaxial cell near its inner conductor and derive deterministic equations of its motion on the basis of the Euler-Lagrange theorem. The potential energy of the model molecule includes the terms determined by the interaction with the electric field in the coaxial cell and by van der Waals' and image charge forces near the conductor walls. In Section 3, a relationship for the AC field gradient force acting on the dipoles is analytically derived in an original pseudo-nonadiabatic approximation, and variations of the translational and angular velocities observed in simulations are explained using a proposed statistical approach. Section 4 is focused on the details and results of the simulation and main trends in the simulated dynamics. Section 5 concludes the paper and outlines some new possible technical applications of the obtained results and nanocoaxes.

2. Modelling Dipole Dynamics in AC Electric Field of a Coaxial Cell

Let a model dipolar diatomic molecule consisting of two masses m_1 and m_2 separated from their centre of mass by l_1 and l_2 and carrying point charges $-q$ and $+q$, respectively, be placed in a coaxial line with a single-wall nanotube as the inner conductor (Figure 1a,b). The field inside the coaxial is inversely proportional to the distance r from its axis

$$\mathbf{E} = \mathbf{a}_r U_0 \Big/ \left[r \ln\left(R_0 / a \right) \right] \qquad (1)$$

where $\mathbf{a}_r$ is the unit radius-vector in polar coordinates, U_0 is the electric potential difference applied to the inner and outer conductors, a and R_0 are the radius of the inner conductor and the inner radius of the outer grounded conductor, respectively. The field outside the coaxial tube is zero. In a general case, static and alternating electric fields can be applied to the conductors. A distribution of electric potential calculated with Comsol Multiphysics® software tool in this coaxial is shown in Fig. 1c with its highest gradient close to the central nanoconductor.

In Figure 1(a), a dipolar molecule is shown in three dimensions in the coaxial tube. Because the molecule is assumed linear and rigid, five generalised coordinates are needed to determine its location in space. If one employs two spherical coordinate systems, then the global coordinates (ρ, θ, and ϕ) describe the location of the centre of mass of the molecule, while the two spherical angles (θ' and ϕ') of the local coordinate system determine the position of the molecular axis. The chemical bond length is assumed constant, so the radial coordinate in the local system is not required. For clarity, the two Cartesian systems are shown in the Figure, with the *z*-axes being parallel to the rotational symmetry axis and the origins of the global and local systems located in the poles of the corresponding spherical systems. The axes of the Cartesian systems are pairwise parallel. The polar axes of the spherical systems lie on the Cartesian *x*-axes.

[Figure 1a,b near here]

[Figure 1c near here]

The geometry of this coaxial tube determines the axially-symmetric one-dimensional spatial non-uniformity of the field and, consequently, the pronounced translational acceleration of the dipolar molecules towards the conductors, which is in the main focus of this work.

To derive the equations of motion, one can take advantage of the Euler-Lagrange equations:

$$\frac{\mathrm{d}}{\mathrm{d}t}\left(\frac{\partial L}{\partial \dot{x}_i}\right)=\frac{\partial L}{\partial x_i} \tag{2}$$

where t is time, x_i and $\dot{x}_i$ are, respectively, the i-th generalised coordinate and its time derivative, and L is the Lagrangian defined as the difference of the total kinetic (T) and potential (U) energies:

$$L = T - U \tag{3}$$

When both rotational and translational dynamics are involved, the kinetic energy of the molecule in the spherical coordinates is

$$T = m\left(\dot{\rho}^2+\rho^2\dot{\theta}^2+\rho^2\dot{\phi}^2\sin^2\theta\right)\Big/2 + I\left(\dot{\theta}'^2+\dot{\phi}'^2\sin^2\theta'\right)\Big/2 \tag{4}$$

where m and I are the mass and moment of inertia of the molecule and the dotted variables are the time derivatives of the corresponding coordinates.

2.1. Potential energy of dipole

The potential energy U can be represented as a sum of four terms, which correspond to the interactions of the electric field with the permanent dipole charges (dipole orientation energy U_d) and with the induced dipole moment (instantaneous polarisation energy U_i) and to the interaction of the dipole with the conductor material (the energy of van der Waals' interactions U_{vdW} and the image charge interaction energy U_{im}):

$$U = U_d + U_i + U_{vdW} + U_{im}. \tag{5}$$

These terms are expanded below.

2.1.1. Interaction of permanent and induced dipole moments with the electric field

As generally known, the electric potential in a point inside a coaxial cable is proportional to logarithm of the distance from the axis to this point. Then, the potential energy of the permanent and induced dipoles in the electric field of the coaxial cable is

$$U_d + U_i = \frac{qU_0 \ln(r_1/r_2)}{\ln(R_0/a)} - \frac{1}{2}\mathbf{E}^* \cdot \boldsymbol{\sigma} \cdot \mathbf{E} \tag{6}$$

where $\mathbf{E}$ and $\mathbf{E}^*$ are the electric field vector and its complex conjugate, $\boldsymbol{\sigma}$ is the molecular polarisability tensor, and r_1, r_2 are the distances of the two charged point masses from the coaxial cell axis, which are expressed in terms of the generalised coordinates as

$$\begin{aligned} r_1 &= \sqrt{(\rho\sin\theta\cos\phi - l_1\sin\theta'\cos\phi')^2 + (\rho\sin\theta\sin\phi - l_1\sin\theta'\sin\phi')^2} \\ r_2 &= \sqrt{(\rho\sin\theta\cos\phi + l_2\sin\theta'\cos\phi')^2 + (\rho\sin\theta\sin\phi + l_2\sin\theta'\sin\phi')^2}. \end{aligned} \tag{7}$$

The second term in (6) accounts for the interaction of the field with the induced dipole moment [51], [52].

Let the voltage difference between the conductors oscillate harmonically with the magnitude V_0, the circular frequency ω, and the phase shift φ_0. Taking into account the relationship for the electric field from (1) and assuming, for simplicity, the molecular polarisability to be isotropic with the localisation at the molecular centre of mass, the first two terms in (5) can then be rewritten as

$$U_d + U_i = q\Phi_0\cos(\omega t + \varphi_0)\ln(r_1/r_2) - \sigma\Phi_0^2\cos^2(\omega t + \varphi_0)/(2r^2), \tag{8}$$

in which the reduced amplitude voltage $\Phi_0 = V_0 / \ln(R_0/a)$ is introduced.

The reduced amplitude voltage Φ_0 is the single dynamics-governing parameter that allows disregarding in calculations specific values of conductors' radii, relating them to the voltage between the conductors. For example, a dipole in two coaxial nanocables with the 2-nm radius of the inner conductor in equal initial conditions (distance from the axis, orientation and velocities) will exhibit the same dynamics if the radii of the outer conductors are 50 and 100 nm and voltage differences are 150 and 182.3 V, respectively.

In the infinitesimal point-dipole approximation, the conditions of $l_1 \ll \rho$ and $l_2 \ll \rho$ are applied. When rearranging the ratio of the distances (7) the logarithm in the first term in (8) and leaving out the terms of the second order of smallness, one arrives at

$$\begin{aligned} U_d &\approx q\Phi_0 \cos(\omega t + \varphi_0) \ln\left[1 - \frac{(l_1 + l_2)\sin\theta'}{\rho \sin\theta} \cos(\phi - \phi')\right] \\ &\approx -p\Phi_0 \cos(\omega t + \varphi_0) \sin\theta' \cos(\phi - \phi') / r \end{aligned} \tag{9}$$

where $p = q(l_1 + l_2)$ is the molecular dipole moment and $r = \rho \sin\theta$ is the distance from the axis to the molecular centre of mass.

It is easy to see that $p \sin\theta' \cos(\phi - \phi') = p_r$ in (9) is the radial component of the vector dipole moment. Then, with taking into account the relationship (1) for the electric field, the classical formula for the potential energy of a point dipole in an arbitrary electric field can be obtained:

$$U_d \approx -\mathbf{p} \cdot \mathbf{E}(r) \tag{10}$$

which confirms the validity of the infinitesimal dipole approximation in the particular case of the interaction with non-uniform electric field of the axial symmetry, provided the distance from the axis to the molecular centre of mass is much larger than the size of the dipolar molecule.

2.1.2. Van der Waals' interaction

The third term in (5), U_{vdW}, can be any conventional two-body interaction potential, such as the Lennard-Jones or Morse potentials. It is often convenient to use a continual approximation of the total van der Waals energy comprised of contributions of all atoms constituting the solid conductor.

In the case of interaction of a molecule with the cylinder surface, it is difficult, although not impossible, to find an exact form of this energy in the continual approximation. As a tenable option, the inner conductor's cylindrical surface with sufficiently large radius a can be imitated with two infinite parallel planes at the distance $2a$ from each other. Let the two-body interaction of n-th atom in the dipole molecule with an atom in the conductor surface separated from each other by distance y_n be described with the Lennard-Jones potential [53]

$$U_{LJ,n} = 4\varepsilon_{LJ,n}\left[\left(\sigma_{LJ,n}/y_n\right)^{12} - \left(\sigma_{LJ,n}/y_n\right)^{6}\right] \quad (11)$$

For the 'right' and 'left' planes imitating the surface of the inner conductor, e. g. of a conductive SWCN, with a wall of atomic thickness one obtains

$$\begin{aligned} y_{n,right}^2 &= \left(r_n - a\right)^2 + x^2 + z^2 \\ y_{n,left}^2 &= \left(r_n + a\right)^2 + x^2 + z^2 \end{aligned} \quad (12)$$

where $n = 1,2$ for the binary molecule and r_n are taken from (7).

In the continual approximation, the full van der Waals energy from atoms of the inner conductor's surface should be sought by integrating the two-body interaction energy $U_{LJ,n}$ with respect to the elementary surface $\mathrm{d}x\mathrm{d}z$ with the surface density of atoms ρ_s [53], i.e.

$$\begin{aligned} U_{vdW} &= 4\rho_s \sum_{n=1,2} \varepsilon_{LJ,n} \Bigg\{ \sigma_{LJ,n}^{12} \int_{-\infty}^{\infty} \mathrm{d}z \int_{-\infty}^{\infty} \left[(r_n - a)^2 + x^2 + z^2 \right]^{-6} \mathrm{d}x - \\ &- \sigma_{LJ,n}^{6} \int_{-\infty}^{\infty} \mathrm{d}z \int_{-\infty}^{\infty} \left[(r_n - a)^2 + x^2 + z^2 \right]^{-3} \mathrm{d}x + \sigma_{LJ,n}^{12} \int_{-\infty}^{\infty} \mathrm{d}z \int_{-\infty}^{\infty} \left[(r_n + a)^2 + x^2 + z^2 \right]^{-6} \mathrm{d}x \\ &- \sigma_{LJ,n}^{6} \int_{-\infty}^{\infty} \mathrm{d}z \int_{-\infty}^{\infty} \left[(r_n + a)^2 + x^2 + z^2 \right]^{-3} \mathrm{d}x \Bigg\} \\ &= 8\pi\rho_s \sum_{n=1,2} \varepsilon_{LJ,n} \left[\frac{\sigma_{LJ,n}^{12}}{10(r_n - a)^{10}} - \frac{\sigma_{LJ,n}^{6}}{4(r_n - a)^{4}} + \frac{\sigma_{LJ,n}^{12}}{10(r_n + a)^{10}} - \frac{\sigma_{LJ,n}^{6}}{4(r_n + a)^{4}} \right]. \end{aligned} \tag{13}$$

In the discrete-site approach, the corresponding energy can exactly be found from the infinite summation over all site-site interactions:

$$U_{vdW} = 4 \sum_{n=1,2} \varepsilon_{LJ,n} \left[\sigma_{LJ,n}^{12} \sum_{i,j,k} \delta_{nijk}^{-12} - \sigma_{LJ,n}^{6} \sum_{i,j,k} \delta_{nijk}^{-6} \right] \tag{14}$$

where δ_{nijk} is the distance between n-th molecular site and an atom with coordinates $(x_{ijk}, y_{ijk}, z_{ijk})$ in the lattice of the inner conductor. In the particular case of the binary molecule in the plane perpendicular to the axis, it is

$$\delta_{nijk} = \sqrt{\left[(-1)^n l_n \sin\varphi + x_{ijk} \right]^2 + \left[(-1)^n l_n \cos\varphi + r - y_{ijk} \right]^2 + z_{ijk}^2}\,. \tag{15}$$

In practice, the summation in (14) should be cut off after the energy contributions of a limited number of least remote atoms of the conductor have been included.

The same energy contribution as in (14) can be obtained for the van der Waals' interactions with the material of the outer conductor, but if the molecule is at much longer distance from it than from the inner conductor, this contribution can be neglected.

2.1.3. Image charge interaction

Fictitious image charges are commonly used to account for interactions of charged particles with conductive materials, in which the charges induce polarisation of the electron density. From electrostatics, the interaction energy of charges $q_i,\ldots,q_j,\ldots$ with the coordinates $(x_i,y_i,z_i),\ldots,(x_j,y_j,z_j)$,… located above a conducting surface [54] is

$$U_{im}=-\frac{1}{8\pi\varepsilon_0}\sum_{i,j}q_iq_j\Big/\sqrt{\left(x_i+x_j-2x_0\right)^2+\left(y_i-y_j\right)^2+\left(z_i-z_j\right)^2} \qquad (16)$$

where x_0 is the coordinate of the conductive surface boundary parallel to yz-plane and ε_0 is the dielectric permittivity of vacuum.

It is possible to extend this formalism to the interaction energy of the dipole in close vicinity of the inner conductor of the coaxial line. In this approach, the surface of the inner conductor is assumed flat. The rotation of the xy-plane about the z-axis through the angle ϕ (Figure 1), with the x-axis becoming normal to the conductive surface, leads to the following formula:

$$\begin{aligned}U_{im}=-\frac{q^2}{16\pi\varepsilon_0}\Bigg\{&\frac{1}{(r-a)-l_1\sin\theta'\cos(\phi-\phi')}+\frac{1}{(r-a)+l_2\sin\theta'\cos(\phi-\phi')}-\\&-4\Big/\sqrt{\left[2(r-a)+\Delta l\sin\theta'\cos(\phi-\phi')\right]^2+l^2\left[\cos^2\theta'+\sin^2\theta'\sin^2(\phi-\phi')\right]}\Bigg\}\end{aligned} \qquad (17)$$

where $\Delta l=l_2-l_1$ and $l=l_2+l_1$.

In the point-dipole approximation, the image charge energy (17) reduces to

$$U_{im} \approx -\frac{p^2\left[1+\sin^2\theta'\cos^2\left(\phi-\phi'\right)\right]}{64\pi\varepsilon_0\left(r-a\right)^3} \tag{18}$$

The relationships for the energy of the image charge interaction with the outer conductor will be similar to those in (17), (18) with the distance $\left(R_0-r\right)$ entering instead of $\left(r-a\right)$. At much longer distances of the dipole from the outer conductor, however, this energy can be ignored.

The equation (18) demonstrates that the dipole image force is always attractive. Together with the van der Waals force, it contributes to formation of adsorbed layer of dipolar molecules on uncharged conductive surfaces.

2.2. Equations of motion

To derive the full system of equations of motion, one should differentiate the Lagrangian (3) containing the kinetic energy (4) and potential energy (5) with its terms specified in (8), (13) and (17) with respect to the five coordinates. Then, according to the Euler-Lagrange theorem (2), the five velocity derivatives of the Lagrangian should be differentiated with respect to time and equated to the corresponding coordinate derivatives. This straightforward operation results in a system of five second-order nonlinear differential equations, which are not spelt out here because of their cumbersomeness.

The numerical integration of this analytically unsolvable system is a rather time-consuming task, especially when using accurate variable-step differential equation solvers. To simplify this problem, one should take into consideration the axial symmetry of the field, which generates one-dimensional non-uniformity along the radial coordinate. In such fields, the adiabatic dynamics of dipolar molecules in two and three dimensions are very similar [55], [56]. This implies that for obtaining correct dynamical characteristics for a molecule, it would be sufficient to consider its motion in a plane perpendicular to the z-axis, thereby reducing the number of the angular coordinates in both systems to one. This single angular coordinate is the angle φ between the field direction and the dipole moment (Figure 1(b)). The neglect of the polar angle θ' is reasonable because the electric field in the plane of θ' variations is uniform and it does not give rise to any translational acceleration of the dipoles. The dipole pendulum dynamics [57], [58] associated with the variation of this angle is observed in the plane of electric field non-uniformity as well, and it does not add any qualitatively new information on the motion of the dipoles in a coaxial line.

When deriving the simplified system of equations of motion, let the polar axis of the coordinate system pass through the centre of mass of the molecule. Then $\theta = \theta' = \pi/2$, $\phi = 0$ and $\phi' = \phi - \varphi = -\varphi$. The distances (7) from the coaxial line axis to the point masses are reduced to

$$\begin{aligned} r_1 &= \sqrt{(r - l_1\cos\varphi)^2 + l_1^2\sin^2\varphi} = \sqrt{r^2 - 2rl_1\cos\varphi + l_1^2} \\ r_2 &= \sqrt{(r + l_2\cos\varphi)^2 + l_2^2\sin^2\varphi} = \sqrt{r^2 + 2rl_2\cos\varphi + l_2^2}, \end{aligned} \tag{19}$$

and the kinetic energy (4) is

$$T = m\dot{r}^2/2 + I\dot{\varphi}^2/2. \tag{20}$$

It is seen that van der Waals' and the image charge interactions are significant only near the conductor surface, in effect, within the length of several angstroms, and they vanish much faster with radial coordinate than the field-determined potential energy variations do. In this work, the detailed dynamics of the dipoles in close vicinity of the conductors is not scrutinised, and the potential energies U_{vdW} and U_{im} are neglected in the calculations.

After the substitution of (19) into the potential function (8), the application of the Euler-Lagrange theorem results in the following equations of motion:

$$\begin{cases} m\ddot{r} + p\Phi_0 \cos\left(\omega t + \varphi_0\right)\dfrac{r\left(l_2 - l_1\right) + \left(r^2 - l_1 l_2\right)\cos\varphi}{r_1^2 r_2^2} + \dfrac{\sigma\Phi_0^2}{r^3}\cos^2\left(\omega t + \varphi_0\right) + \\ + \dfrac{\partial U_{vdW}\left(r,\varphi\right)}{\partial r} + \dfrac{\partial U_{im}\left(r,\varphi\right)}{\partial r} = 0, \\ I\ddot{\varphi} + pr\Phi_0 \cos\left(\omega t + \varphi_0\right)\sin\varphi \dfrac{r^2 + l_1 l_2}{r_1^2 r_2^2} + \dfrac{\partial U_{vdW}\left(r,\varphi\right)}{\partial \varphi} + \dfrac{\partial U_{im}\left(r,\varphi\right)}{\partial \varphi} = 0. \end{cases} \tag{21}$$

These equations represent a scalar form of Newton's second law for the radial translational and rotational motion of the dipole.

It is worthwhile to note that the system (21) in the point-dipole approximation of $l_1 \,\square\, l_2 \,\square\, \left(r \approx r_1 \approx r_2\right)$ is reduced to a couple of equations that encompass the translational motion driven by the classical gradient force [59] and the angular nonlinear-pendulum-like motion [58] in the first terms in the right-hand sides:

$$\begin{cases} m\ddot{\mathbf{r}} = \left[\left(\mathbf{p} + \sigma\mathbf{E}\left(r\right)\right)\cdot\nabla\right]\mathbf{E}\left(r\right) - \nabla_r U_{vdW} - \dfrac{3p^2\left[1 + \cos^2\varphi\right]}{64\pi\varepsilon_0\left(r-a\right)^4}\mathbf{a}_r, \\ I\ddot{\boldsymbol{\varphi}} = \mathbf{p}\times\mathbf{E}\left(r\right) + \nabla_\varphi U_{vdW}\times\mathbf{a}_r + \mathbf{p}\times\left(\mathbf{p}\cdot\mathbf{a}_r\right)\mathbf{a}_r \Big/ \left[64\pi\varepsilon_0\left(r-a\right)^3\right]. \end{cases} \tag{22}$$

The more concise potential energy gradient form of the van der Waals terms is employed in (22) to evade cumbersome notation in terms of the dipole moment and radial distance.

In the simulations and analytical derivations, the form (21) is used with the short-range van der Waals and image charge contributions omitted.

3. Analytical Approach to the Nonlinear Dynamics of a Polarisable Dipole in the Potential of a Coaxial Cell

Although the system of equations (21) can be solved numerically, the resulting solution can hardly provide any information on patterns of dynamics of dipolar rotators in the coaxial line. Moreover, the numerical solving of these equations is a time-consuming task, largely due to the presence of the sinusoidal function of the angular coordinate entering in the second equation of the system (21), and alternative approaches for fast calculations are needed. In this Section, a relationship for the radial force driving the dipoles towards or away from the nanosized inner conductor of a coaxial is obtained. In addition, approximate formulas for the radial translational and angular velocities are derived on the basis of simple energy conservation principles.

When considering the system (21) in the point dipole approximation, the finite size of the dipole can be neglected so that $l_1 \approx l_2 \approx 0$ and $r_1 \approx r_2 \approx r$. Taking into account that the field gradient is $\mathrm{d}E/\mathrm{d}r = -\Phi_0 \cos\left(\omega t + \varphi_0\right)/r^2$, the first equation in (21) with the neglected surface forces is reduced to

$$m\ddot{r} = -\frac{p\Phi_0}{r^2}\cos\left(\omega t + \varphi_0\right)\cos\varphi - \frac{\sigma\Phi_0^2}{r^3}\cos^2\left(\omega t + \varphi_0\right), \tag{23}$$

which is equivalent to a familiar expression of the gradient force acting on a dipole [52], [59]:

$$\mathbf{F}_{grad} = \left[\left(\mathbf{p} + \sigma\mathbf{E}\right)\cdot\nabla\right]\mathbf{E}\left(x, y, z, t\right) \tag{24}$$

where the vector sum of the permanent and induced dipole moments is put in the parentheses.

Thus, the sign of the gradient force along the radius of the coaxial line, i.e. the direction of the force vector, depends on the sign of $\cos(\omega t+\varphi_0)\cos\varphi$.

The presence of $\cos\varphi$ in (23) makes it coupled to the angular coordinate equation from the system (21). Knowing the dependence of φ on time and radial coordinate, one can arrive at a single independent equation for r. This decoupling can be done, under certain assumptions, as described below.

3.1. Angular coordinate relationships

Consider the second equation from (21) in the point-dipole approximation:

$$\ddot{\varphi}=-\frac{p\Phi_0}{Ir}\cos(\omega t+\varphi_0)\sin\varphi. \tag{25}$$

The solution of this equation is known to involve the deterministic chaos (stochasticity) [60], [61], which means that after a certain length of time the solution will no longer be predictable. The stochasticity is established at the timescale of a field oscillation period [62], whereas at shorter periods the angle variation is purely deterministic.

Let the angular coordinate φ in (25) be regarded as a simple sum of a large-amplitude (φ_l) and a small-amplitude (φ_s) components:

$$\varphi=\varphi_l+\varphi_s. \tag{26}$$

The large-amplitude angular coordinate is related to either the chaotic (stochastic) oscillations or rotation, and the small-amplitude component appears as a purely deterministic result of librational motion in the strong-field areas. The small-amplitude librational angle φ_s is assumed to be close to zero when $\cos(\omega t+\varphi_0)\geq 0$ or close to π when $\cos(\omega t+\varphi_0)<0$.

The chaotic large-amplitude component results from the nonlinearity in the right side of (25), whereas the deterministic angular coordinate is supposed to be small ($\varphi_s \ll \varphi_l$), and it contributes to the linear variations of the angle φ. Then, the expansion of $\sin\varphi$ into a Taylor series in the vicinity of φ_l gives

$$\sin\varphi \approx \sin\varphi_l + \varphi_s \cos\varphi_l . \tag{27}$$

If the small-amplitude acceleration is dominant and the equations of the type (25) with equipartitioned initial angles are being solved, the mean large-amplitude component contribution in (27) can be eliminated by angle averaging. Two different situations need to be considered in this connection.

The condition of the free dipole rotation, when the mean kinetic energy of the angular motion $I\langle\dot{\varphi}\rangle_0^2/2$ is much larger than the potential energy barrier $2p\Phi_0\left|\cos\left(\omega t+\varphi_0\right)\right|/r$, suggests that the angle averaging should be performed over the range from $-\pi$ to $+\pi$. Here, $\langle\dot{\varphi}\rangle_0$ denotes the mean angular velocity of the dipoles in the zero-field conditions (at large enough distances from the axis).

On the other hand, if the free rotation condition is not satisfied, the chaotic angle averaging will apply. The chaotic variation of this angle implies de-correlation from the field and deterministic angle oscillations, so the chaotic angle functions can be averaged separately in the equations of motion. Taking into consideration that the energy width of the stochastic layer near the separatrix is in the order of the halved potential barrier [60], which corresponds to the angle variation of $\pm\pi/2$ from the potential minimum, the chaotic angle averaging should be performed over the angle interval from $-\pi/2$ to $+\pi/2$. Hence, at sufficiently high driving frequencies ($\omega \gtrsim 10^{10}$ rad·s^{-1})

$$\langle \sin\varphi \rangle_{\varphi_l} \approx \begin{cases} \dfrac{1}{\pi}\displaystyle\int_{-\pi}^{+\pi} \sin\varphi_l' \mathrm{d}\varphi_l' + \dfrac{\varphi_s}{\pi}\displaystyle\int_{-\pi}^{+\pi} \cos\varphi_l' \mathrm{d}\varphi_l' = 0, \text{ if } \langle \dot\varphi \rangle_0^2 \gg \dfrac{4p\Phi_0 \left|\cos(\omega t + \varphi_0)\right|}{Ir}, \\ \dfrac{1}{\pi}\displaystyle\int_{-\pi/2}^{+\pi/2} \sin\varphi_l' \mathrm{d}\varphi_l' + \dfrac{\varphi_s}{\pi}\displaystyle\int_{-\pi/2}^{+\pi/2} \cos\varphi_l' \mathrm{d}\varphi_l' = \dfrac{2\varphi_s}{\pi}, \text{ otherwise.} \end{cases}$$

(28)

Taking (26) and (28) into account, the equation (25) with a multitude of initial conditions can be expanded into a pair of equations containing the large- and small-amplitude angle variables:

$$\begin{cases} \ddot\varphi_l = 0, \\ \ddot\varphi_s = -2\varphi_s p\Phi_0 \cos(\omega t + \varphi_0)/(\pi I r). \end{cases} \quad (29)$$

From the averaging, the initial angle in the first equation in (29) is zero and

$$\varphi_l = \upsilon t \quad (30)$$

where υ is the angular drift velocity, which is associated with either the rotation or chaotic angular drift over relatively long-time periods. In strong fields, the angular drift velocity depends on the radial distance from the axis, as discussed in Section 3.4. In weak fields, it is assumed to be the mean rotational velocity $\langle \dot\varphi \rangle_0$ of gas molecules, which depends only on temperature according to the Maxwell statistics.

Consider now the second equation in (29). Although this is a special case of the Mathieu equation, and it can be exactly solved in terms of the Mathieu functions [63], in this study it is approximately solved using the above-mentioned small-amplitude angle approach.

Let the main-mode oscillation be much faster than the field alternation, so that $\cos(\omega t + \varphi_0)$ and r are nearly constant. Then, the second equation in (29) is reduced in this approximation to

$$\ddot{\varphi}_s + \omega_0^2 \varphi_s = 0 \tag{31}$$

where $\omega_0^2 = p\Phi_0 \left|\cos\left(\omega t + \varphi_0\right)\right| / \left(Ir\right)$.

When averaging the cosine in this relationship over different phases, one arrives at

$$\omega_0^2 = 2p\Phi_0 / \left(\pi I r\right). \tag{32}$$

The solution of the linear differential equation (31) is found separately for the weak-field and strong-field conditions. The definition of these conditions is given below in (34). The weak-field solution is supposed to be trivial ($\varphi_s = 0$), because the angle variation is mainly caused by rotation.

The strong-field solution of (31) is found using the initial conditions of an arbitrary initial oscillation phase φ_a: $\varphi_s\left(0\right) = \mathrm{A}\cos\varphi_a$ and $\dot{\varphi}_s\left(0\right) = -\mathrm{A}\sin\varphi_a / \omega_0$ at $t = 0$. The amplitude A is derived from the full energy conservation equation:

$$1 - \cos\mathrm{A} = \dot{\varphi}_{\max}^2 / \left(2\omega_0^2\right) \tag{33}$$

where $\dot{\varphi}_{\max}$ is the maximum angular velocity of the dipole librations.

Because of the linearity of (31), the librational angular velocity varies harmonically, hence the mean squared angular velocity is $\langle\dot{\varphi}^2\rangle = \dot{\varphi}_{\max}^2 / 2$. Therefore, the solution of (31) is

$$\varphi_s \approx \begin{cases} \arccos\left[1 - \langle\dot{\varphi}^2\rangle / \left(4\omega_0^2\right)\right]\cos\left(\omega_0 t + \varphi_a\right), & \text{if } \langle\dot{\varphi}^2\rangle \le 8\omega_0^2, \\ 0, & \text{if } \langle\dot{\varphi}^2\rangle > 8\omega_0^2, \end{cases} \tag{34}$$

where ω_0 is defined in (32).

Then, taking into consideration (26), (30), and (34),

$$\varphi \approx \begin{cases} \arccos\left[1-\pi\langle\dot{\varphi}^2\rangle Ir \big/ \left(8p\Phi_0\right)\right]\cos\left(\omega_0 t+\varphi_a\right)+\upsilon t, & \text{if } \langle\dot{\varphi}^2\rangle \le 8\omega_0^2, \\ \upsilon t, & \text{if } \langle\dot{\varphi}^2\rangle > 8\omega_0^2. \end{cases} \tag{35}$$

The averaging of the squared time derivative of (35) results in an equation with the variable $\langle\dot{\varphi}^2\rangle$:

$$\langle\dot{\varphi}^2\rangle = \begin{cases} \dfrac{1}{2}\omega_0^2 \arccos^2\left[1-\langle\dot{\varphi}^2\rangle \big/ \left(4\omega_0^2\right)\right]+\upsilon^2, & \text{if } \langle\dot{\varphi}^2\rangle \le 8\omega_0^2, \\ \upsilon^2, & \text{if } \langle\dot{\varphi}^2\rangle > 8\omega_0^2. \end{cases} \tag{36}$$

If $\langle\dot{\varphi}^2\rangle \ll 8\omega_0^2$, the squared arc cosine may be expanded in a Taylor series near $\langle\dot{\varphi}^2\rangle \big/ \left(4\omega_0^2\right) = 0$. If it is truncated after the second term, the first equation in (36) can be rearranged into the quadratic one:

$$\langle\dot{\varphi}^2\rangle = \langle\dot{\varphi}^2\rangle/4 + \langle\dot{\varphi}^2\rangle^2 \big/ \left(96\omega_0^2\right) + \upsilon^2 . \tag{37}$$

The solution of (37), combined with the weak-field counterpart from (36), is

$$\langle\dot{\varphi}^2\rangle = \begin{cases} 36\omega_0^2\left(1-\sqrt{1-2\upsilon^2 \big/ \left(27\omega_0^2\right)}\right), & \text{if } \omega_0^2 \ge 3\upsilon^2/16, \\ \upsilon^2, & \text{if } \omega_0^2 < 3\upsilon^2/16. \end{cases} \tag{38}$$

Finally,

$$\varphi \approx \begin{cases} \arccos\left(1-\mathrm{B}\right)\cos\left(\omega_0 t+\varphi_a\right)+\varphi_l, & \text{if } \omega_0^2 \ge 3\upsilon^2/16, \\ \varphi_l, & \text{if } \omega_0^2 < 3\upsilon^2/16, \end{cases} \tag{39}$$

where

$$\mathrm{B} = 9\left(1 - \sqrt{1 - 2\upsilon^2 / \left(27\omega_0^2\right)}\right). \quad (40)$$

3.2. AC field gradient force in the attraction and repulsion translational regimes

The analytical expression for the force driving the dipole to or from the inner cylinder of the coaxial is given in (23). As mentioned, decoupling the translational motion equation from the angle variable requires an explicit formulation of $\cos\varphi$ in (23) as a function of time and radial coordinate. A good approximation of $\cos\varphi$ inferred from (39) is

$$\cos\varphi \approx \begin{cases} \left[1 - \mathrm{B}\cos^2\left(\omega_0 t + \varphi_a\right)\right]\cos\varphi_l - \sin\left[\arccos\left(1-\mathrm{B}\right)\cos\left(\omega_0 t + \varphi_a\right)\right]\sin\varphi_l, & \\ & \text{if } \omega_0^2 \geq 3\upsilon^2/16, \\ \cos\varphi_l, & \text{if } \omega_0^2 < 3\upsilon^2/16. \end{cases} \quad (41)$$

The averaging over the large-amplitude angle φ_l, by analogy with (28), and over the initial phase φ_a of the dipole librations in (41) yields

$$\cos\varphi \approx \begin{cases} \left(2-\mathrm{B}\right)/\pi, & \text{if } \omega_0^2 \geq 3\upsilon^2/16, \\ 0, & \text{if } \omega_0^2 < 3\upsilon^2/16. \end{cases} \quad (42)$$

After the substitution of (32), (40) and (41) into (23) and averaging over the initial field phase φ_0, the following expression for the AC field gradient force acting on a dipole in the coaxial potential can be obtained:

$$m\ddot{r} = \begin{cases} \mp\dfrac{4p\Phi_0}{\pi^2 r^2}\left[1 - \dfrac{9}{2}\left(1 - \sqrt{1 - \pi I r\upsilon^2/\left(27p\Phi_0\right)}\right)\right] - \dfrac{\sigma\Phi_0^2}{2r^3}, & \text{if } \upsilon^2 \leq \dfrac{32p\Phi_0}{3\pi I r} \\ -\sigma\Phi_0^2/\left(2r^3\right), & \text{otherwise.} \end{cases} \quad (43)$$

The minus sign in the first term of (43) accounts for the attraction of a dipole to the inner conductor, and the plus corresponds to the dipole repulsion mode. In the given approximation, the dipole force is frequency-independent unlike the ponderomotive force acting on a solitary charge [64].

Thus, the most essential modification of the gradient force in (43) is the introduction of the phase-averaging factor $2/\pi$ and the dipole orientation factor (42). They are valid for any type of potential if corresponding corrections in the libration frequency ω_0 and angular drift velocity υ are made. The angular drift velocity also contributes to the establishment of the attraction or repulsion translational regimes, as discussed below.

3.3. The cut-off translational velocity and mean translational velocities in the attraction and repulsion regimes as the initial parameters for solving (43)

The fact that dipoles can be ejected out of non-uniform electric fields in the adiabatic limit was emphasised in [56]. It was found that the ejection occurs if the translational energy normalised by the full Hamiltonian is below some critical value, y_{0c}, which is functionally related to the normalised critical potential energy, x_c, decelerating the dipole to a standstill:

$$y_{0c} = 1 - 2K\left(k_c\right) \Big/ \left(\pi^2 x_c\right) \tag{44}$$

where K is the complete elliptic integral of the first kind, and its argument $k_c = 0.9089$ is found from the equation

$$K\left(k_c\right) = 2E\left(k_c\right), \tag{45}$$

with E being the complete elliptic integral of the second kind.

The adiabatic critical translational and potential energies are, respectively, $y_{0c,a} = 0.2879$ and $x_{c,a} = 1.533$.

If the initial potential energy is small enough, the condition for a plane rotator to be ejected out of the stronger field gradients is expressed in the following inequality:

$$T_{rot}/T_{tr} > (1 - y_{0c})/y_{0c} \quad (46)$$

where T_{rot} and T_{tr} are the initial rotational and translational energies, respectively.

In the perfectly nonadiabatic limit, use of this approach suggests that the critical potential energy needed to stop the molecules is the adiabatic one reduced by the phase-averaging factor $2/\pi$: $x_{c,na} = x_{c,a}\pi/2 = 2.408$. Then, the perfectly nonadiabatic critical translational energy from (44) is $y_{0c,na} = 0.5467$.

In the adiabatic and perfectly nonadiabatic limits, the ratios of the rotational and translational energies from the ejection condition (45) should be greater than 2.4734 and 0.8293, respectively. Apparently, in between these limits, the critical ratio of the kinetic energies varies with the field strength and frequency. Finding this dependence is difficult, and we take advantage of a naïve assumption that the actual nonadiabatic critical ratio is simply the arithmetic mean of these two values: $T_{rot}/T_{tr} > \chi_{na}$ where $\chi_{na} = (2.4734 + 0.8293)/2 = 1.6514$. This inequality imposes the limit on the initial translational velocity above which the dipoles are attracted and below which they are repelled by the field. From the equipartition of kinetic energy over the degrees of freedom, this mean cut-off velocity is

$$v_c = \langle \dot{\varphi} \rangle_0 \sqrt{I/(\chi_{na} m)} \quad (47)$$

where $\langle\dot{\varphi}\rangle_0$ is the mean initial rotational velocity. Considering, in general, the existence of three non-degenerated rotational degrees of freedom, $\langle\dot{\varphi}\rangle_0$ can be found from the Maxwell distribution as the square root of one third of the mean squared rotational velocity:

$$\langle\dot{\varphi}\rangle_0 = \sqrt{\frac{4\pi}{3}\left(\frac{I}{2\pi k_B T}\right)^{3/2}\int_0^\infty w^4 \exp\left(-\frac{Iw^2}{2k_B T}\right)\mathrm{d}w} = \sqrt{k_B T/I} \qquad (48)$$

Then, from the Maxwell distribution one can construct two individual distribution functions for the initial velocities of the field-attracted and repelled dipoles. The modified distribution function for the translational velocity of the attracted dipoles is

$$f_{in}(v) = \frac{4\pi\left(\frac{m}{2\pi k_B T}\right)^{3/2} v^2 \exp\left(-\frac{mv^2}{2k_B T}\right)}{1-\mathrm{erf}\left(v_c\sqrt{\frac{m}{2k_B T}}\right)+v_c\sqrt{\frac{2m}{\pi k_B T}}e^{-\frac{mv_c^2}{2k_B T}}}, \qquad (49)$$

and that of the repelled ones is

$$f_{ex}(v) = \frac{4\pi\left(\frac{m}{2\pi k_B T}\right)^{3/2} v^2 \exp\left(-\frac{mv^2}{2k_B T}\right)}{\mathrm{erf}\left(v_c\sqrt{\frac{m}{2k_B T}}\right)-v_c\sqrt{\frac{2m}{\pi k_B T}}e^{-\frac{mv_c^2}{2k_B T}}}. \qquad (50)$$

The normalizing factors (the denominators) in (49) and (50) warrant that the integrals of these functions over the velocity ranges from zero to v_c and from v_c to infinity, respectively, are equal to unity.

Hence, by analogy with the mean rotational velocity (48), the mean initial translational one of the field-attracted dipoles is

$$v_{in} = -\sqrt{(1/3)\int_{v_c}^{\infty} v^2 f_{in}(v)\mathrm{d}v}\,, \tag{51}$$

and that of the field-repelled dipoles is

$$v_{ex} = -\sqrt{(1/3)\int_{0}^{v_c} v^2 f_{ex}(v)\mathrm{d}v}\,. \tag{52}$$

At 393 K, their values are –447 m·s^{-1} and –146 m·s^{-1}, respectively. These velocities are used as the initial parameters when solving (43) separately for the attraction and repulsion regimes. The equation of motion is numerically integrated using the Adams-Bashforth-Moulton algorithm embedded in Matlab, with the absolute and relative tolerances 10^{-6}. In Figure 3(a) the three lines represent the results of solving (43) with the three reduced voltages, and in Figure 3(b) the corresponding solutions are shown as numbered solid lines.

3.4. Mean angular velocities in the attraction and repulsion regimes

To find the angular velocities of the dipole in the repulsion and attraction regimes, it is necessary first to determine the limiting radial coordinate $r_{\lim}$ at which the dipole can be ejected out of the field gradient.

Let the dipoles travel to the inner conductor with some variable angular drift velocity υ. The travel direction is reversed when the potential energy U is at its extreme. This potential energy can be found from integration of the right-hand side of (43), taken with the opposite sign, with respect to the radial coordinate. For the strong field case, it is

$$U(r) = \mp \frac{4p\Phi_0}{\pi^2 r}\left[\frac{9}{2}\left(1-\sqrt{1-\frac{\pi I r \upsilon^2}{27p\Phi_0}}+\frac{\pi I r \upsilon^2}{27p\Phi_0}\operatorname{arctanh}\sqrt{1-\frac{\pi I r \upsilon^2}{27p\Phi_0}}\right)-1\right]-\frac{\sigma\Phi_0^2}{r^2} \quad (53)$$

where the minus-plus sign has the same meaning as in (43).

Equating the strong-field force in (43) to zero and, for the sake of simplicity, neglecting the polarisation term, one can yield the solution for r_{lim}:

$$r_{\mathrm{lim}} \approx 77p\Phi_0 \big/ \left(3\pi I \upsilon^2\right). \quad (54)$$

The angular drift velocity υ, yet undefined, should be sought as the initial angular velocity of the dipoles travelling between r_{lim} and the radius a of the inner conductor. Here, it is found the arithmetic mean of the minimum and maximum initial angular velocities at which the statistically-averaged switch of the dipole travel direction can occur:

$$\upsilon = \left(\langle\dot{\varphi}\rangle_{\mathrm{lim}} + \langle\dot{\varphi}\rangle_{\mathrm{max}}\right)\big/2 \quad (55)$$

The limiting angular velocity $\langle\dot{\varphi}\rangle_{\mathrm{lim}}$, below which the dipole is not repelled by the field, is found from (38), with $\langle\dot{\varphi}\rangle_0$ entering as the angular drift velocity:

$$\begin{aligned}\langle\dot{\varphi}\rangle_{\mathrm{lim}} &= \sqrt{\frac{72p\Phi_0}{\pi I r_{\mathrm{lim}}}\left(1-\sqrt{1-\pi I r_{\mathrm{lim}}\langle\dot{\varphi}\rangle_0^2\big/\left(27p\Phi_0\right)}\right)} \\ &\approx \upsilon\sqrt{\frac{216}{77}\left(1-\sqrt{1-\frac{77}{216}\left(\langle\dot{\varphi}\rangle_0/\upsilon\right)^2}\right)}\end{aligned} \quad (56)$$

In other words, $\langle\dot{\varphi}\rangle_{\mathrm{lim}}$ is the border line which separates the rotational (the weak-field case) and field-induced stochastic angular (the strong-field case) drift velocities stipulated in Eq.(30) and the following equations.

The maximum velocity $\langle\dot{\varphi}\rangle_{\max}$ is determined from the sum of the mean kinetic energy of the angular motion at $r_{\lim}$ and one quarter of the potential energy difference between $r_{\lim}$ and a (because the equipartitioned translational and rotational energies are supposed to be stored in the potential energy in equal amounts, and only one half of the latter accounts for the period-averaged kinetic energy), i.e.

$$\langle\dot{\varphi}\rangle_{\max} = \sqrt{\langle\dot{\varphi}\rangle_{\lim}^2 + \frac{2p\Phi_0}{\pi^2 I}\left[\Xi(a) - \Xi(r_{\lim})\right]} \tag{57}$$

where

$$\Xi(r) = \frac{1}{r}\left[1 - \frac{9}{2}\left(1 - \sqrt{1 - \frac{\pi I r \upsilon^2}{27 p\Phi_0}} + \frac{\pi I r \upsilon^2}{27 p\Phi_0}\operatorname{arctanh}\sqrt{1 - \frac{\pi I r \upsilon^2}{27 p\Phi_0}}\right)\right] \tag{58}$$

To circumvent the difficulty of solving the complex system of equations (54)-(58), the self-consistent calculation of $r_{\lim}$, $\langle\dot{\varphi}\rangle_{\lim}$, and $\langle\dot{\varphi}\rangle_{\max}$ can be performed in an iterative manner.

After the repulsion, the dipole will keep rotating at the minimum angular velocity $\langle\dot{\varphi}\rangle_{\lim}$ beyond $r_{\lim}$ because the weak field will no longer influence it. Hence, from the conservation of rotational energy, the mean rotational velocity $\langle\dot{\varphi}\rangle_{0,ex}$ needed for the dipole to be repelled from the inner conductor is calculated from the sum of the rotational energy corresponding to the limiting angular velocity $\langle\dot{\varphi}\rangle_{\lim}$ and the mean rotational energy for all velocities above $\langle\dot{\varphi}\rangle_{\lim}$. The latter is found from the modified Maxwell distribution in the same manner as it is done for the mean translational velocity in (49) and (51):

$$\langle\dot{\varphi}\rangle_{0,ex} = \sqrt{\langle\dot{\varphi}\rangle_{\lim}^2 + \frac{\frac{4\pi}{3}\left(\frac{I}{2\pi k_B T}\right)^{3/2}\int_{\langle\dot{\varphi}\rangle_{\lim}}^{\infty} w^4 \exp\left[-\frac{Iw^2}{2k_B T}\right]\mathrm{d}w}{1-\operatorname{erf}\sqrt{\frac{I\langle\dot{\varphi}\rangle_{\lim}^2}{2k_B T}} + \sqrt{\frac{2I\langle\dot{\varphi}\rangle_{\lim}^2}{\pi k_B T}}\exp\left[-\frac{I\langle\dot{\varphi}\rangle_{\lim}^2}{2k_B T}\right]}}. \quad (59)$$

It is obvious in the framework of the current approach that there is virtually no upper limit for the initial angular velocity of the dipoles attracted to the inner conductor. Therefore, their mean initial rotational velocity is

$$\langle\dot{\varphi}\rangle_{0,in} = \langle\dot{\varphi}\rangle_0. \quad (60)$$

The mean angular velocities of the attracted dipoles calculated from (57) for the three reduced voltages are plotted as lines in Figure 4(a). In Figure 4(b), the mean initial and final velocities of the field-repelled dipoles calculated from (59) and (56) are shown as circles and crosses, respectively. The velocity variations with the reduced voltage are so small that the corresponding symbols overlap with each other.

4. Simulation

4.1. Simulation details

The realistic values of the dipole moment and polarisability in (21) are adopted to be those of a water molecule ($p = 1.85$ D=$6.17\cdot10^{-30}$ C·m and $\sigma = 1.607\cdot10^{-40}$ F·m^2, respectively). The point masses are equal to those of an oxygen atom on its negative end (m_1=$2.65602\cdot10^{-26}$ kg) and two hydrogen atoms on its positive end (m_2=$3.34707\cdot10^{-27}$ kg). The total mass entering into (21) is $m = m_1 + m_2$. The distance l_1 from the negative end to the centre of mass is $6.507\cdot10^{-12}$ m, and the distance l_2 is found from the balance of the masses

$$m_1 l_1 = m_2 l_2 . \tag{61}$$

Because the main goal of this study is to demonstrate the specific mechanisms of velocity variation for a free dipole in the non-uniform electric field, special requirements are imposed on the initial distance between the dipole and the inner conductor's surface. It should be no larger than the mean free path in the rarefied medium. In this regime, the deterministic motion, unaffected by binary collisions, is dominant. Furthermore, it is assumed that the electric field does not essentially alter the initial thermal equilibrium velocities, which are set randomly according to the Maxwell distribution.

Generally, the mean free path of a molecule in a gas is found [65] as

$$\lambda = M \Big/ \left(\sqrt{2} \pi d_{eff}^2 \rho N_A \right) \tag{62}$$

where M and ρ are the molar mass and density of the gas, d_{eff} =1.92·10^{-10} m is the effective collision diameter [66], and N_A is Avogadro's constant. With the initial temperature T_0 =393 K, the initial distance is taken to be $\lambda = 3.23 \cdot 10^{-7}$ m, which corresponds to the mean free path of water vapour molecules at ambient pressure. The dipoles in the simulations start in a radial direction towards the inner conductor, i.e. their initial translational velocities are negative.

In studying effects of alternating electric fields, four reduced amplitude voltages (15, 60, 90, and 150 V) and two field frequencies (10^{10} and 10^{12} rad·s^{-1}) are employed. The 150-V field is involved only in the qualitative characterisation of the dipole migration in the subsection below. The total effect of the electric fields is derived from the averaging of dynamic characteristics over eight uniformly-spaced field phases (0, $\pi/4$, $\pi/2$,…, $7\pi/4$).

The distance from the inner and outer conductor is assumed long enough so that the short-range surface forces (Sections 2.1.2 and 2.1.3) are not taken into account in the simulations.

The number of samplings is limited to 110 events of attraction to the conductor.

4.2. Two patterns of the free dipole migration: field attraction and repulsion

Preliminary simulation results manifest two different trends of the dipole migration in the electric field of the coaxial (Figure 2) in the free-molecular limit. The dipoles can be either attracted to the inner conductor with strong non-uniformity of the field or repelled from it. The fractions of the field-repelled dipoles at 393 K are 0.39-0.45 and 0.27-0.4 at the frequencies 10^{10} and 10^{12} rad·s^{-1}, respectively, and they decrease with the voltage increase.

The realisation of either the attractive or repulsive regime depends on a number of factors, such as the initial translational and angular velocities and coordinates of the dipolar molecule and the parameters of the alternating field. It is difficult to predict all the initial conditions that will definitely lead to the field attraction or repulsion, the final velocities, and dipole travel times. Yet, a statistical analysis of dynamics of many dipoles with random initial angles and initial velocities sampled from the Maxwell distribution will yield the average dynamic characteristics of the dipolar molecules in the coaxial. Below, we focus on dependence of the mean translational and angular velocities on the reduced voltages and radial distances.

[Figure 2 near here]

4.3. Translational and angular velocities

In the simulations, dynamic characteristics of the molecules in the attraction and repulsion events are considered separately. The simulation results for the repulsion events are time-averaged, whereas in the case of attraction, the results are averaged at specific radial coordinates (10, 7, 5, and 2 nm).

In Figure 3(a), the translational velocities of dipoles attracted by the non-uniform field are plotted against the radial coordinate as discrete symbols. In the fields of given parameters, this velocity increases with the radial coordinate decrease, and it grows almost linearly with the reduced voltage. At the same time, the change in the field frequency from 10^{10} to 10^{12} rad·s^{-1} has no or little effect on the velocity variation. The solutions of (43) for the attraction regime follow the simulation points almost perfectly, except for very small radial distances, where the effects of dipole's finite length are appreciable.

The time-averaged translational velocities of the dipoles ejected out of the field are shown in Figure 3(b). In this regime, the solutions of (43) differ from the simulation results the more significantly, the smaller the radial coordinate, especially in the case of low voltages. This discrepancy is caused by the neglect of the dipole gradient force for the weak field conditions laid in the basis of the analytical approach. Nonetheless, the conservation of the translational energy in the repulsion mode is correctly reproduced in the solutions of (43) and in the simulation results.

A noteworthy feature in the simulation results in Figure 3 is that the mean initial translational velocities are higher in the attraction regime (about 485 m·s^{-1}) and lower in the repulsion mode (about 150 m·s^{-1}) than the Maxwell distribution value, which is taken as the square root of one third of mean squared velocity (392 m·s^{-1} at 393 K). This feature reflects the correspondence of the two regimes to the different areas of the translational velocity in the Maxwell distribution which are separated with the cut-off velocity. These mean velocities prove to be in close agreement with the analytical results (51) and(52).

The absolute values of angular velocities of the dipoles in both regimes are depicted in Figure 4. It is seen that the simulated angular velocity in the attraction regime (Figure 4(a)) rises with the radial coordinate decrease and tends to saturation with the reduced voltage increase. The agreement with the analytical calculation is quite fair, but the discrepancy progressively rises with the field strength. It reaches 24% for the radial distance 2 nm and reduced amplitude voltage 90 V. The reason for this disaccord is the influence of the polarisation term neglected in (57)-(58), which decreases the angular velocity while increasing the translational one. One can also notice that the calculated initial angular velocities at $r = \lambda$ are somewhat higher than those obtained from the simulations and given in (60) because the weak-field conditions are disregarded in the derivation of (57).

The mean rotational velocity of dipoles in the field repulsion regime is shown in Figure 4 (b). It is seen that before the repulsion the dipoles rotate at constant velocities up to reaching a certain radial distance, below which the velocities drop with r and remain constant after the repulsion. The simulated initial and final rotational velocities are in agreement with the analytical estimates from (59) and (56) within an accuracy of 8% and 11%, respectively.

[Figure 3a near here]

[Figure 3b near here]

[Figure 4a near here]

[Figure 4b near here]

As an important conclusion, the initial velocities determine the attractive or repulsive regime of dipole migration in the time-varying non-uniform electric fields in the classical dynamics approximation. This outcome cancels the Maxwellian statistics of initial velocities of the molecules in both regimes, except for the initial rotational velocity in the attraction mode. Moreover, the non-uniform AC fields break the adiabatic invariance of the mean angular momentum [55], [56] of the dipolar molecules, imparting additional angular acceleration to the attracted dipoles and slowing down the rotation of the repelled ones.

5. Conclusions and Implications for Future Research

In this work, the classical dynamics of a linear dipolar rotator in a strongly non-uniform AC electric field near a conducting nanotube as the inner conductor of a coaxial cable has been considered both analytically and in simulations. The developed model is applicable to classical dynamics calculation at fields of increased frequencies as well, i.e. of the microwave, infrared, optical and optical-plasmonic ranges. The potential energy used in the derivation of equations of motion has been considered as a sum of four components: the energy of the permanent and induced dipoles in electric field, the van der Waals energy of interaction with the material of the conductor, and the image charge energy accounting for polarisation of conductor's surface.

In the developed analytical pseudo-nonadiabatic approach, the nonlinear equations of motion have been decoupled upon an assumption of the angular coordinate composed of the small- and large-amplitude angles, averaging with respect to the latter, and separation of the angular coordinate equations for the weak-field (almost purely rotational dynamics) and the strong-field regions (librational and chaotic dynamics). This approach has allowed us to ultimately arrive at a relationship (43) for the AC field gradient force acting on a dipole in a coaxial, which shows the dynamic characteristics of the field-attracted dipoles to be in very good agreement with the simulation results.

It is noteworthy that the proposed approach is valid for predicting dipole dynamics in non-uniform fields of not only nanocoaxes but also macroscopic coaxial cells. In the latter case, for tangible influence on the translational dynamics of dipoles, the voltage between the conductors must be megavolts or higher in order to produce the comparable field gradient magnitudes at the commensurate gas temperatures.

By analogy with the adiabatic approach [56], it has been suggested that the ratio of translational and rotational velocities of the dipole travelling to the inner conductor is the main factor determining the dynamic regimes of field-induced attraction or repulsion. This ratio has been obtained in the semi-nonadiabatic approximation. The consequence of this relationship is the existence of the cut-off translational velocity separating the initial velocities of the field-attracted and -repelled molecules in the Maxwell distribution, and it has explained velocity differences observed in the simulations.

The rotational velocities of the molecules that can be repelled by the field have proven to have a lower limit. Above this limit, the mean angular velocities of either attracted or repelled dipoles in the strong fields have been analytically calculated from the energy conservation considerations, and the comparison of the analytical and simulation results has been made.

The simulations based on the equations of motion have revealed existence of the two different dynamic regimes, in line with the analytical results. The initial translational and rotational velocities of the field-attracted and repelled dipoles has proven to differ from their average Maxwellian values, which indicates the separation of dipoles according to their velocities in these regimes. It has been established that the mean initial translational velocities of the attracted and repelled dipoles are, respectively, higher and lower than the average. The mean initial rotational velocity of the repelled dipoles is higher than the Maxwellian average, and that of the attracted ones is nearly equal to it.

In the attraction regime, both the translational and angular velocities increase as the molecules approach the inner nanotube conductor. This increase has been found to be the more pronounced, the greater the reduced voltage amplitude on the coaxial. In the repulsion regime, the magnitudes of the translational velocity are conserved and the rotational velocity is decreased upon the repulsion, exhibiting minor dependence on the reduced voltage. The field frequencies have proven to have little influence on the dynamics of the free dipoles in both regimes.

The results obtained in this work offer possibility of designing new types of gas heating and cooling devices. The drastic increase of the translational and angular velocities of dipolar molecules in AC fields near nanosized conductors provides strong temperature increase in the adjacent areas of gas volume. On the other hand, gaseous medium made up of spatially isolated field-repelled molecules, whose kinetic energy is lower than the average one, can serve as a refrigerant. Such separation can be realised, for instance, using flat arrays of field-polarised nanotube (nanowire) conductors with the spacing of the order of $2r_{\lim}$. The field-attracted molecules will rebound from the surface of the nanotubes, whereas some fraction of the non-attracted molecules will pass through the gaps. Series of such arrays can give rise to a considerable temperature drop.

The results obtained in this work are applicable to chemical synthesis as well. The increased kinetic energy of dipoles attracted to the nanosized conductor in AC electric fields raises the local temperature, thereby facilitating overcoming the activation energy barrier and accelerating chemical reactions, both catalyzed and non-catalyzed, on the surface of these conductors.

Another possible application, which can be useful in precise spectroscopic measurements and collisional studies, is the development of dipole traps and angular velocity selectors in analogy to the well-known translational-velocity separators [67],

[68]. The underlying operating principle, similar to that proposed in [69]-[74], is the equilibration of the force (43) at a fixed voltage magnitude and the centrifugal force acting on molecules tangentially injected in a coaxial. If the frequency of molecular collisions is negligibly small, the molecules will orbit around the inner conductor at radii corresponding to their initial rotational velocities. After partitioning in a coaxial cell according to the angular velocities, the molecules can be released through an annular slit, cut in the outer conductor, by gradually decreasing the voltage magnitude.

The results of this study can find application in development of new methods for separation and identification of molecular species based on the difference in dipolar and higher-order electric moments, moments of inertia, and polarisabilities of the molecules. As it follows from (43), the dipole moment and polarisability are the main properties controlling the attractive force in the regions of relatively large and small radial coordinate, respectively. The increase of the voltage magnitude will force the molecules orbiting around the inner conductor to shift to the axis the closer, the greater their dipole moment or polarisability. The angular velocities and moments of inertia are the factors of lesser importance in this displacement. If the loading of the coaxial cell with molecules is not too high, the molecular species can be fully separated. This separation technique can be a viable alternative to the evolving methods of the optical force chromatography [75], which are based on the similar principles.

For the chemical identification, the locations of separate radial density maxima should be explored by means of an auxiliary method, e. g. recording of the ion current of laser-induced ionisation. If the angular velocity distribution is known, the combination of dipole moment, polarisability, and moment of inertia determining the radial coordinate of each peak will give a unique ‘fingerprint’ of each molecular species.

Acknowledgements

Authors greatly appreciate the access to the high-performing computing facilities granted by the Norwegian Metacenter for Computational Science (Notur).

Funding details

One of the authors (S. Kapranov) acknowledges the Ph.D. scholarship granted by Research Council of Norway, Grant IME-055, and partial financial support within the state assignment AAAA-A18-118021350003-6 from Kovalevsky Institute of Marine Biological Research of Russian Academy of Sciences.

Disclosure statement

No potential conflict of interest was reported by the authors

References

[1] S.H. Petrosko, R. Johnson, H. White and C.A. Mirkin, J. Am. Chem. Soc. **138**(24), 7443-7445 (2016). doi:10.1021/jacs.6b05393

[2] S.A. Miners, G.A. Rance and A.N. Khlobystov, Chem. Soc. Rev. **45**(17), 4727-4746 (2016). doi:10.1039/c6cs00090h

[3] M.T. De Martino, L.K.E.A. Abdelmohsen, F.P.J.T. Rutjes and J.C.M. Hest, Beilstein J. Org. Chem. **14**, 716-733 (2018). doi:10.3762/bjoc.14.61

[4] Z. Wang, X. Lv, Y. Chen, D. Liu, X. Xu, G.T.R. Palmore and R.H. Hurt, Nanoscale **7**(22), 10267-10278 (2015). doi:10.1039/c5nr00963d

[5] U.H. Brinker and J.-L. Mieusset, editors, *Molecular Encapsulation: Organic Reactions in Constrained Systems* (Wiley, Hoboken, 2010).

[6] S.V. Kapranov and G.A. Kouzaev, Surf. Sci. **667**, 66-78 (2018). doi:10.1016/j.susc.2017.09.004

[7] J. Hu, Y. Bando, J. Zhan, C. Zhi, and D. Golberg, Nano Lett. **6**(6), 1136-1140 (2006). doi:10.1021/nl060245v

[8] V. Van Meervelt, M. Soskine, S. Singh, G.K. Schurman-Wolters, H.J. Wijma, B. Poolman and G. Maglia, J. Am. Chem. Soc. **139**(51), 18640-18646 (2017). doi:10.1021/jacs.7b10106

[9] R. Roa, W.K. Kim, M. Kandic, J. Dzubiella and S. Angioletti-Uberti, ACS Catal. **7**(9), 5604-5611 (2017). doi:10.1021/acscatal.7b01701

[10] X. Li, J. Liu, A.F. Masters, V.K. Pareek and T. Maschmeyer, APL Mater. **1**(4), 041101 (2013). doi:10.1063/1.4826155

[11] P.-Y. Bolinger, D. Stamou and H. Vogel, J. Am. Chem. Soc. **126**(28), 8594-8595 (2004). doi:10.1021/ja049023u

[12] L. Daehne, S. Leporatti, E. Donath and H. Moehwald, J. Am. Chem. Soc. **123**(23), 5431-5436 (2001). doi:10.1021/ja002911e

[13] A. Botos, J. Biskupek, T.W. Chamberlain, G.A. Rance, G.T. Stoppiello, J. Sloan, Z. Liu, K. Suenga, U. Kaiser and A.N. Khlobystov, J. Am. Chem. Soc. **138**(26), 8175-8183 (2016). doi:10.1021/jacs.6b03633

[14] D.S. Talaga and J. Li, J Am. Chem. Soc. **131**(26), 9287-9297 (2009). doi:10.1021/ja901088b

[15] K.J. Freedman, M. Jurgens, A. Prabhu, C.W. Ahn, P. Jemth, J.B. Edel and M.J. Kim, Anal. Chem. **83**(13), 5137-5144 (2011). doi:10.1021/ac2001725

[16] Bekard and D.E. Dunstan, Soft Matt. **10**(3), 431-437 (2014). doi:10.1039/c3sm52653d

[17] A. Amadei and P. Marracino, RCS Adv. **5**(117), 96551-96561 (2015). doi:10.1039/c5ra15605j

[18] R.V. Krems, Int. Rev. Phys. Chem. **24**(1), 99-118 (2005). doi:10.1080/01442350500167161

[19] G. Ying and G.A. Kouzaev, Physica B 499, 87-96 (2016). doi:10.1016/j.physb.2016.07.018

[20] A.P. Fields and A.E. Cohen, Proc. Natl. Acad. Sci. USA **108**(22), 8937-8942 (2011). doi:10.1073/pnas.1103554108

[21] Y. Ai, Z. Zeng and S. Qian, J. Colloid Interface Sci. **417**, 72-79 (2014). doi:10.1016/j.jcis.2013.11.034

[22] X. Pan, Z. Fan, W. Chen, Y. Ding, H. Luo and X. Bao, Nat. Mater. **6**(7), 507-511 (2007). doi:10.1038/nmat1916

[23] N. Murakami, Y. Tango, H. Miyake, T. Tajima, Y. Nishima, W. Kurashige, Y. Negishi and Y. Takaguchi, Sci. Rep. **7**, 43445 (2017). doi:10.1038/srep43445

[24] E. Chavazzo, M. Fasano, P. Asinari and P. Decuzzi, Nat. Commun. **5**, 4565 (2013). doi:10.1038/ncomms4565

[25] B. Luan and A. Aksimentiev, J. Phys. Cond. Matt. **22**(45), 454123 (2010). doi:10.1088/0953-8984/22/45/454123

[26] K. Ritos, M.K. Borg, N.J. Mottram and J.M. Reese, Philos. Trans. Royal Soc. A **374**(2060), 20150025 (2016). doi:10.1098/rsta.2015.0025

[27] A. Shahriari, P. Birbah, J. Oh, N. Miljkovic, V. Bahadur, Nanoscale Microscale Thermophys. Eng. **21**(2), 102-121 (2016). doi:10.1080/15567265.2016.1253630

[28] G.-L. Tian, Q. Zhang, B. Zhang, Y.-G. Jin, J.-Q. Huang, D.S. Su and F. Wei, Adv. Funct. Mater. **24**(38), 5956-5961 (2014). doi:10.1002/adfm.201401264

[29] Y. Cheng, S. Zhao, B. Johannessen, J.-P. Veder, M. Saunders, M.R. Rowles, M. Cheng, C. Liu, M.F. Chisholm, R. De Marco, H.-M. Cheng, S.-Z. Yang and S.P. Jiang, Adv. Mater. **30**(13), 1706287 (2018). doi:10.1002/adma.201706287

[30] Y. Lan, Y. Wang and Z.F. Ren, Adv. Phys. **60**(4), 553-678 (2011). doi:10.1080/00018732.2011.599963

[31] S. Cambre, J. Campo, C. Beirnaert, C. Verlackt, P. Cool and W. Wenseleers, Nat. Nanotechnol. **10**(3), 248-252 (2015). doi:10.1038/nnano.2015.1

[32] D.J. Riley. M. Mann, D.A. McLaren, P.C. Dastoor and W. Allison, Nano Lett. **3**(10), 14455-1458 (2003). doi:10.1021/nl034460c

[33] M.M. Archibald, B. Rizal, T. Connoly, M.J. Burns, M.J. Naughton and T.C. Chiles, Biosens. Bioelectron. **74**, 406-410 (2015). doi:10.1016/j.bios.2015.06.069

[34] B. Rizal, M.M. Archibald, T. Connoly, S. Shepard, M.J. Burns, T.C. Chiles and M.J. Naughton, Anal. Chem. **85**(21), 10040-10044 (2013). doi:10.1021/ac402441x

[35] H. Zhao, B. Rizal, G. McMahon, H. Wang, P. Dhakal, T. Kirkpatrck, Z. Ren, T.C. Chiles, M.J. Naughton and D. Cai, ACS Nano **6**(4), 3171-3178 (2012). doi:10.1021/nn205036e

[36] H. Ni, M. Wang, T. Shen and J. Zhou, ACS Nano **9**(2), 1913-1925 (2015). doi:10.1021/nn506834r

[37] G.A. Kouzaev, S.V. Kapranov, UK Patent Application No. GB1504690.7 (19 March 2015); Searchable Patents J. **6644** (21 September 2016).

[38] R. Rizal, J.M. Merlo, M.J. Burns, T.C. Chiles and M.J. Naughton, Analyst **140**(1), 39-58 (2015). doi:10.1039/c4an01447b

[39] M. Chinappi, C.M. Casciola, F. Cecconi, U.M.B. Marconi and S. Melchionna, Europhys. Lett. **108**(4), 46002 (2014). doi:10.1209/0295-5075/108/46002

[40] K. Kim, P. Rice, P. Kabos and D.S. Filipovic, presented at the 2010 IEEE International Symposium on Electromagnetic Compatibility, Fort Lauderdale, FL, USA, 25-30 July 2010, 853-856 (2010). doi:10.1109/isemc.2010.5711391

[41] J. Dahdah, J. Hoblos and F.I. Baida, IEEE Photon. J. **4**(1), 87-94 (2012). doi:10.1109/jphot.2011.2178820

[42] H.J. Kulik, N. Luehr, I.S. Ufimtsev and T. J. Martinez, J. Phys. Chem. B 116(41), 12501-12509 (2012). doi:10.1021/jp307741u

[43] N.J. English and C.J. Waldron, Phys. Chem. Chem. Phys. **17**(19), 12407-12440 (2015). doi:10.1039/c5cp00629e

[44] M. Lemeshko, R. V. Krems, J.M. Doyle and S. Kais, Mol. Phys. **111**(12-13), 1648-1682 (2013). doi:10.1080/00268976.2013.813595

[45] S.V. Kapranov and G.A. Kouzaev, Eur. Phys. J. B **89**, 126 (2016). doi:10.1140/epjb/e2016-70027-5

[46] C.O. Kappe, A. Stadler and D. Dallinger, *Microwaves in Organic and Medicinal Chemistry*, 2nd ed. (Wiley-VCH, Weinheim, 2012). doi:10.1002/9783527647828

[47] A.C. Metaxas and R.J. Meredith, *Industrial Microwave Heating* (IET, London, 2008).

[48] S.V. Kapranov and G.A. Kouzaev, Int. J. Thermal Sci **122**, 53-73 (2017). doi:10.1016/j.ijthermalsci.2017.08.007

[49] J.I. Qureshi, presented at the 9th IEEE International Multitopic Conference IEEE INMIC 2005, Karachi, Pakistan, 24-25 December 2005, 1-3 (2005). doi:10.1109/inmic.2005.334393

[50] S.V. Kapranov and G.A. Kouzaev, Int. J. Thermal Sci. **49**(12), 2319-2330 (2010). doi:10.1016/j.ijthermalsci.2010.07.008

[51] Y. Dodin and N.J. Fisch, Phys. Plasmas **14**(5), 055901 (2007). doi:10.1063/1.2436149

[52] P.C. Chaumet and M. Nieto-Vesperinas, Opt. Lett. **25**(15), 1065-1067 (2000). doi:10.1364/ol.25.001065

[53] J. Israelachvili, *Intermolecular and Surface Forces*, 2nd ed. (Academic Press, London, 1992).

[54] F. Iori and S. Corni, J. Comp. Chem. **29**(10), 1656-1666 (2008). doi:10.1002/jcc.20928

[55] E. Gershnabel and I. Sh. Averbukh, J. Chem. Phys. **134**(5), 054304 (2011). doi:10.1063/1.3535600

[56] V.M. Rozenbaum, Sov. Phys. JETP **76**(4), 589-596 (1993). <http://www.jetp.ac.ru/cgi-bin/dn/e_076_04_0589.pdf>

[57] G.A. Kouzaev, *Applications of Advanced Electromagnetics: Components and Systems* (Springer, Berlin, 2013).

[58] S.V. Kapranov and G.A. Kouzaev, Physica D **252**, 1-21 (2013). doi:10.1016/j.physd.2013.02.007

[59] T. B. Jones, *Electromechanics of Particles* (Cambridge University Press, Cambridge, UK, 1995).

[60] G.M. Zaslavsky, R.Z. Sagdeev, D.A. Usikov and A.A. Chernikov, *Weak Chaos and Quasi-Regular Patterns* (Cambridge University Press, Cambridge, UK, 1991).

[61] A.R. Kolovsky, Phys. Rev. A **51**(5), 4005-4009 (1995). doi:10.1103/PhysRevA.51.4005

[62] S.V. Kapranov and G.A. Kouzaev, presented at the 4th International Conference on Circuits, Systems, Control, and Signals, Valencia, Spain, 6-8 August 2013, 97-101 (2013). doi:10.13140/2.1.4119.9049

[63] N.W. McLachlan, *Theory and Application of Mathieu Functions* (Clarendon Press, Oxford, 1947).

[64] A. Kildal, Contrib. Plasma Phys. **39**(4), 349-358 (1999). doi:10.1002/ctpp.2150390408

[65] J.O. Hirschfelder, C.F. Curtiss and R.B. Bird, *Molecular Theory of Gases and Liquids* (Wiley, New York, 1964).

[66] M. Yao and Y. Hiejima, J. Mol. Liq. **96-97**, 207-220 (2002). doi:10.1016/S0167-7322(01)00349-X

[67] C. Szewc, J.D. Collier and H. Ulbricht, Rev. Sci. Instr. **81**(10), 106107 (2010). doi:10.1063/1.3499254

[68] F. Pirani, D. Cappelletti, F. Vecchiocattivi, L. Vattuone, A. Gerbi, M. Rocca and U. Valbusa, Rev. Sci. Instr. **75**(2), 349-354 (2004). doi:10.1063/1.1637433

[69] H.J. Loesch and B. Scheel, Phys. Rev. Lett. **85**(13), 2709-2712 (2000). doi:10.1103/PhysRevLett.85.2709

[70] S.K. Sekatskiĭ, JETP Lett. **62**(12), 916-920 (1995). <http://www.jetpletters.ac.ru/ps/1223/article_18477.pdf>

[71] R.T. Jongma, G. von Helden, G. Berden and G. Meijer, Chem. Phys. Lett. **270**(3-4), 304-308 (1997). doi:10.1016/S0009-2614(97)00382-5

[72] S.A. Rangwala, T. Junglen, T. Rieger, P.W.H. Pinkse and G. Rempe, Phys. Rev. A **67**(4), 043406 (2003). doi:10.1103/PhysRevA.67.043406

[73] M.R. Tarbutt, H.L. Bethlem, J.J. Hudson, V.L. Ryabov, V.A. Ryzhov, B.E. Sauer, G. Meijer and E.A. Hinds, Phys. Rev. Lett. **92**(17), 173002 (2004). doi:10.1103/PhysRevLett.92.173002

[74] T. Rieger, T. Junglen, S. A. Rangwala, P. W. H. Pinkse and G. Rempe, Phys. Rev. Lett. **95**(17), 173002 (2005). doi:10.1103/PhysRevLett.95.173002

[75] B.S. Zhao, Y.-M. Koo and D.S. Chung, Anal. Chim. Acta **556**(1), 97-103 (2006). doi:10.1016/j.aca.2005.06.065

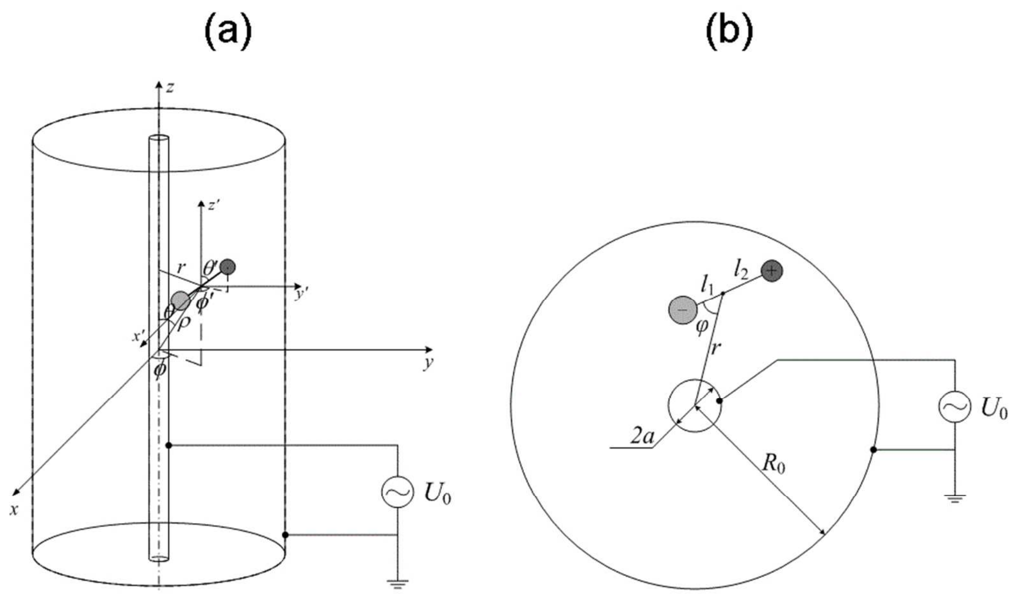

Figure 1. (a) Magnified representation of a dipolar molecule inside a coaxial cell and the coordinates used to describe its spatial location; (b) molecule in a plane perpendicular to the axis of the coaxial cell.

340x200mm (72 x 72 DPI)

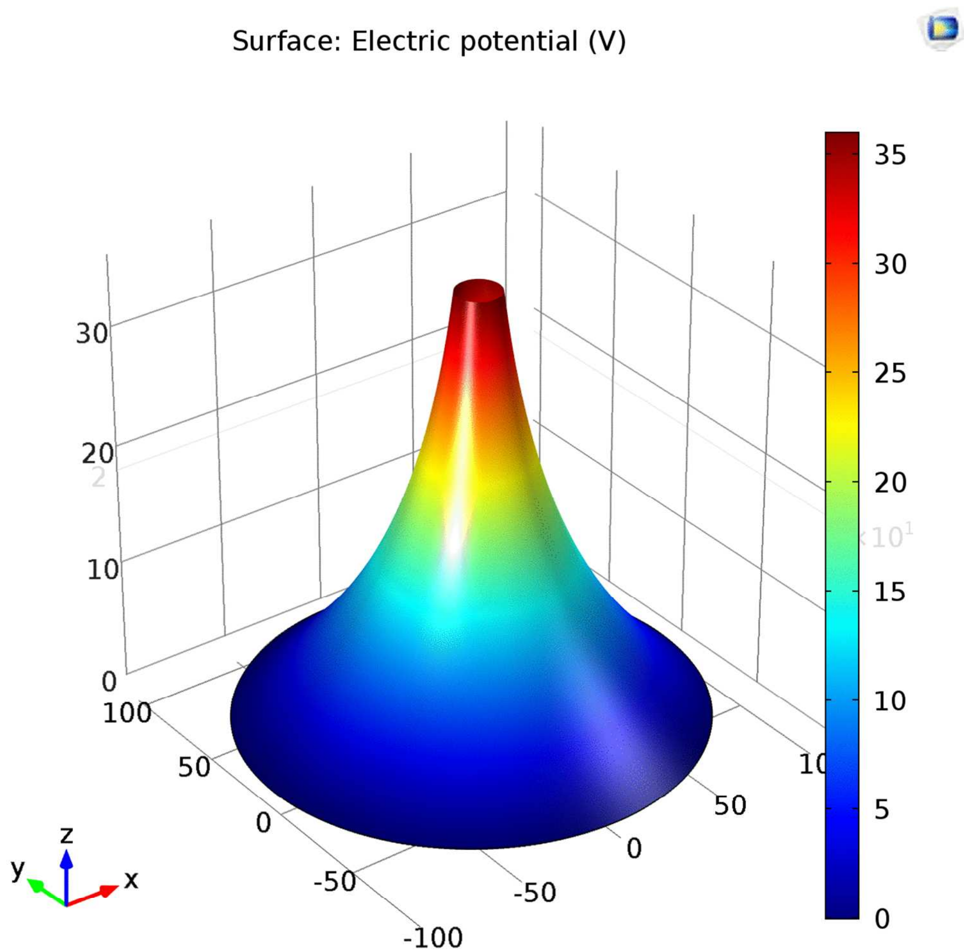

Figure 1. (c) Electric potential distribution in a nanocoaxial cell with a=10 nm, R_0=100 nm, U_0=36 V

499x499mm (72 x 72 DPI)

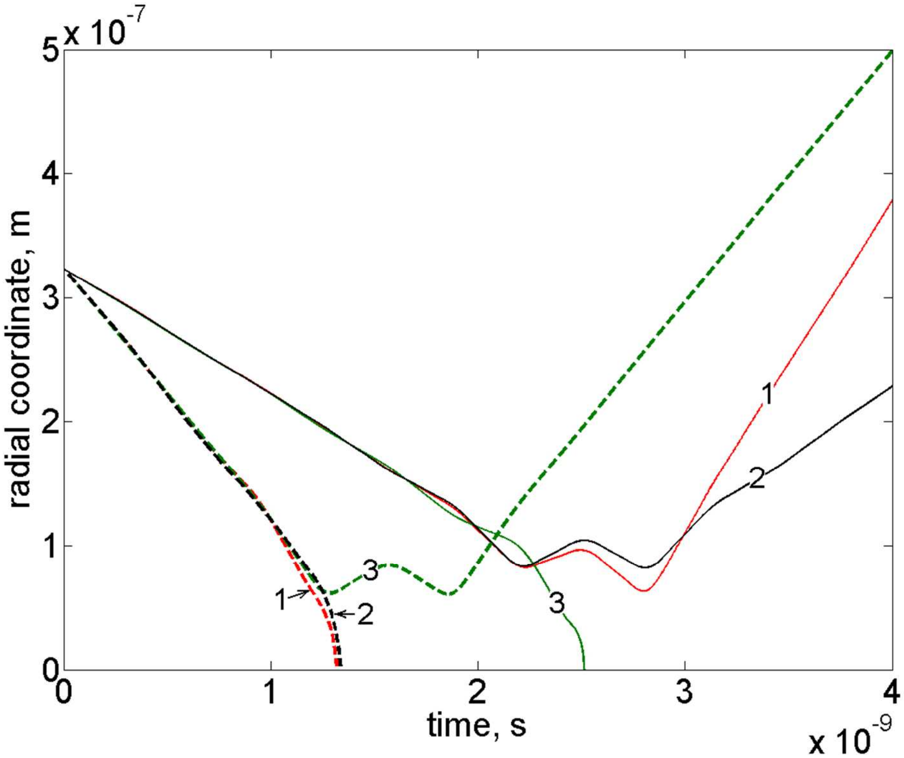

Figure 2. Simulated radial migration of a dipole near the inner conductor with the radius 10 nm at different initial conditions in the alternating electric field with circular frequency 10^{10} rad·s^{-1} and reduced amplitude voltage Φ_0 150 V. The initial angular velocity of the dipoles is $3\cdot10^{13}$ rad·s^{-1} and the initial translational velocities are −100 m·s^{-1} (solid lines) and −200 m·s^{-1} (dashed lines). The initial angles made by the dipole moment with a radius-vector are 0 (red lines, 1), π/2 (black lines, 2), and π (green lines, 3). The initial field phase is zero.

411x313mm (72 x 72 DPI)

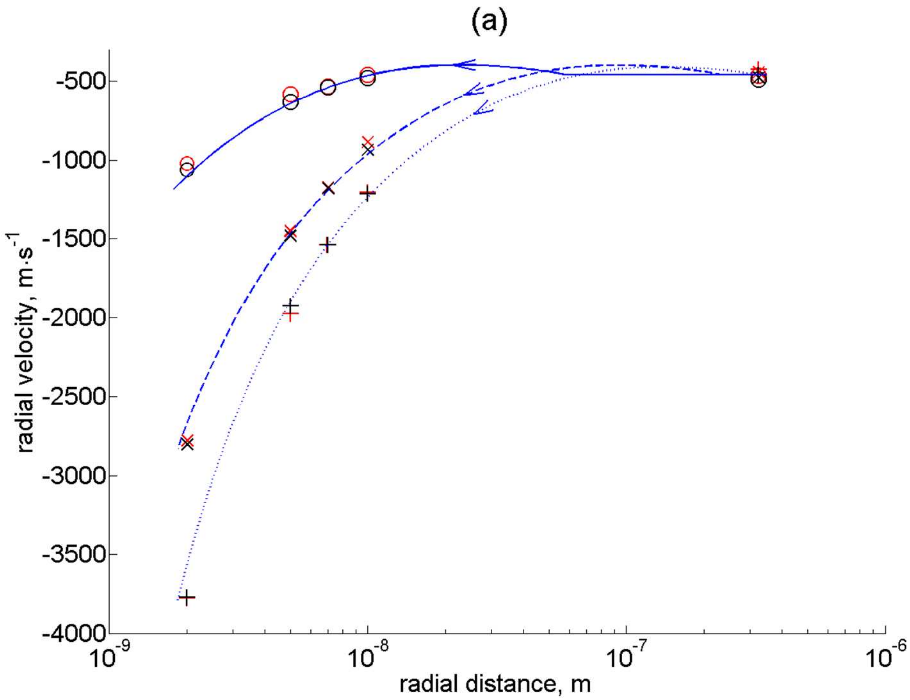

Figure 3. (a) Mean radial translational velocity of the dipoles attracted to the inner conductor. Lines: integration of (43) with the initial velocity (51); symbols: simulation results for $\omega=10^{10}$ (red) and 10^{12} rad·s^{-1} (black); $\Phi\Phi_0$=15 V (circles), 60 V (slanted crosses), 90 V (upright crosses). The arrows denote the direction of the coordinate variation with time.

453x324mm (72 x 72 DPI)

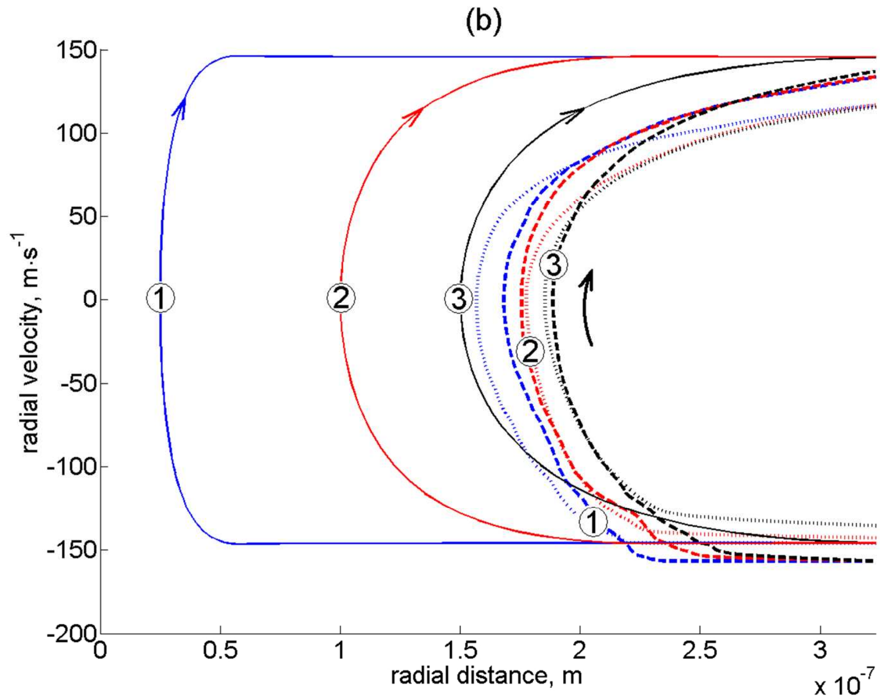

Figure 3. (b) Mean radial translational velocity of the dipoles repelled from the inner conductor. Solid lines: integration of (43) with the initial velocity (52); dashed and dotted lines: simulation results for $\omega=10^{10}$ and 10^{12} rad·s^{-1}, respectively; $\Phi\Phi_0$ =15 V (blue, 1), 60 V (red, 2), 90 V (black, 3). The arrows denote the direction of the coordinate variation with time.

453x324mm (72 x 72 DPI)

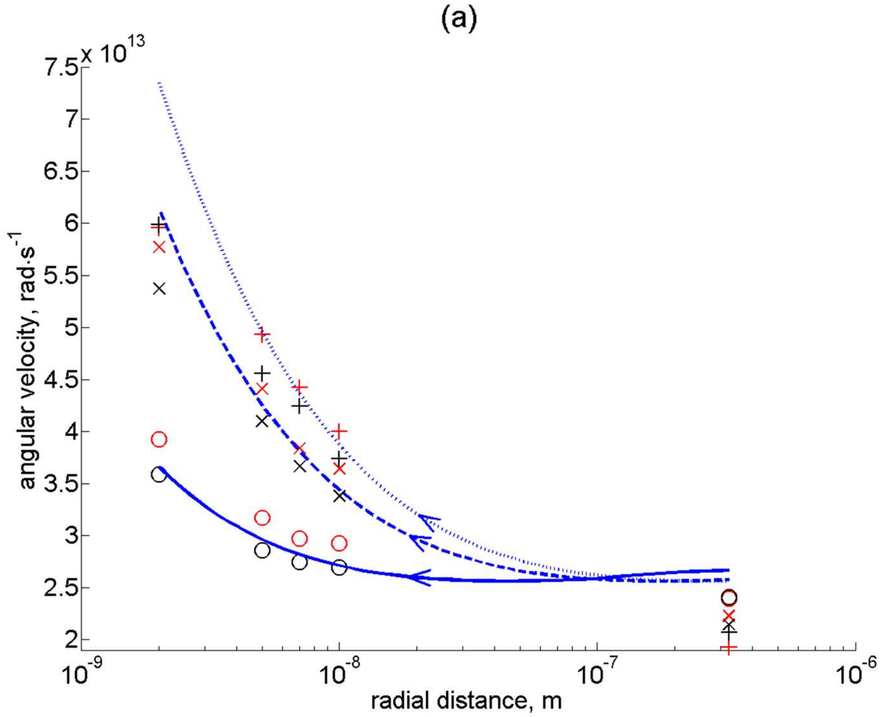

Figure 4 (a) Absolute values of angular velocity of the dipoles attracted to the inner conductor. Lines: analytical calculation from (57)-(58); symbols: simulation results. Line types, symbols and colors correspond to the same field parameters as in Figure 3(a). Circles and crosses: analytical calculation of the mean initial and final velocity from (59) and (56), respectively. The arrows denote the direction of coordinate variation with time.

453x335mm (72 x 72 DPI)

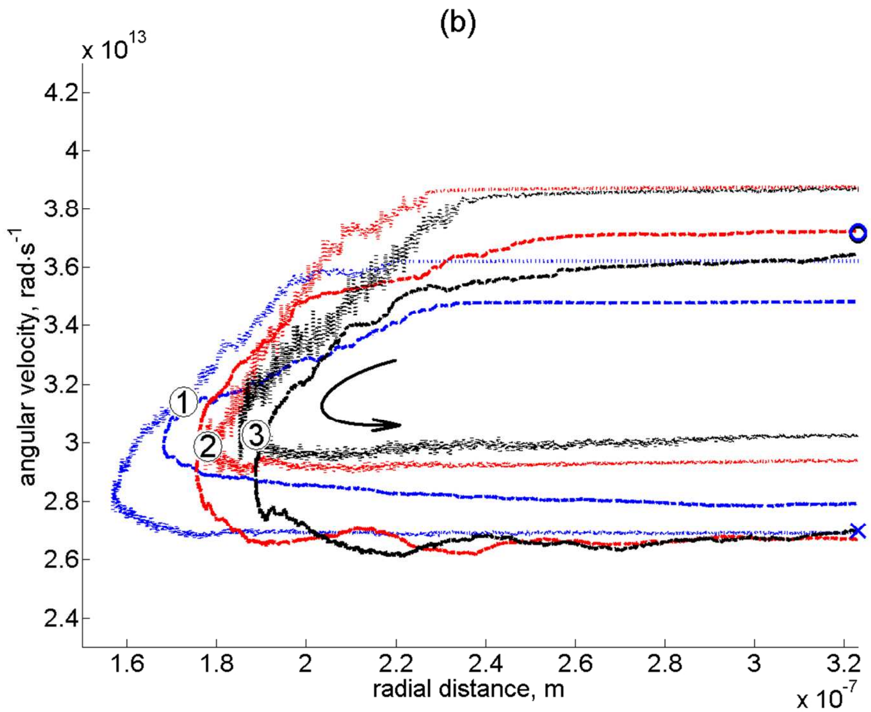

Figure 4. (b) Absolute values of angular velocity of the dipoles (a) attracted to and (b) repelled from the inner conductor. (b) Dashed and dotted lines: simulation results, with the numbers and colors corresponding to those in Figure 3(b). Circles and crosses: analytical calculation of the mean initial and final velocity from (59) and (56), respectively. The arrows denote the direction of coordinate variation with time.

453x335mm (72 x 72 DPI)